Nitrogen Supersaturation into AISI420 Mold for Precise Machining

Tatsuhiko Aizawa[1,a], Hiroshi Morita[2,b]* and Tatsuya Fukuda[3,c]

[1]Surface Engineering Design Laboratory, Tokyo 144-0045, Japan

[2]Nano-Film Coat, llc., Tokyo 144-0045, Japan

[3]Tokai Engineering Service, Co., Ltd., Kyoto 601-8306, Japan

[a]taizawa@sic.shibaura-it.ac.jp, [b, *]hiroshi-m@mtc.biglobe.ne.jp, [c]t-fukuda@tes2001.com

Abstract. The plasma nitriding conditions and processing parameters were controlled to attain the high-density nitrogen ion and NH-radical populations and to form the nitrogen supersaturated layer into AISI420 type martensitic stainless steel mold substrate at 673 K for 14.4 ks and 28.8 ks. Thicker nitrided layer than 80 μm was attained for fine machining of the optical diffraction elements onto this nitrided AISI420 mold surface. The average hardness in this nitrogen supersaturated layer reached 1400 HV. After this hardness testing and microstructure analysis, the machinability test was performed to describe the ductile mode cutting behavior of nitrogen-supersaturated work by using the PCD (Poly-Crystalline Diamond)-chip tool. Higher average nitrogen solute content than 4 mass% was responsible for fine turning by PCD-chip and CVD (Chemical Vapor Deposition)-diamond coated cutting tools without any damages and for precisely finishing the mold surface with the lower maximum surface roughness than 10 nm on the machined mold surface. The low roughness and homogeneous machined surface profile proved that the nitrogen supersaturated AISI420 series stainless steel was adaptive as a stamping mold of chalcogenide glasses with high dimensional accuracy and demolding capacity.

Introduction

The martensitic stainless steel type AISI420 has been widely utilized as a substrate material for hot mold-stamping of oxide and phosphorous glass preforms with relatively high glass-transition temperature. How to form the mold surface with high dimensional accuracy, was high-lighted as a technological issue [1]. The amorphous film coating such as NiP (Nickel Phosphorous) and NiWP (Nickel-Tungsten Phosphorous) films often failed during mold-stamping because of crystallization at the elevated temperature [2]. Instead of those amorphous coating, an alternative surface treatment is needed to have sufficient hardness and chemical inertness during mold stamping, fine machining and finishing processes, and to have fine microstructure with high quality as-finished surface profile.

The conventional plasma nitriding processes [3-4] were the first candidate treatments; the iron and chromium nitride precipitated surface layers must be removed to utilize the nitrogen diffusing zones with lower nitrogen solute content than 2 mass%. The low temperature plasma nitriding [5-7] provides another way to make nitrogen supersaturation without nitride precipitation and to harden the stainless steels; e.g., AISI304 and AISI316 austenitic stainless steels [8-9; 10-11] as well as AISI420 martensitic stainless steels [12-14] were nitrogen-supersaturated with higher nitrogen content than 4 mass%. This high nitrogen solute content in this nitrogen supersaturated layer, prevents the diamond-coated or PCD-chipped tools from severe damages by interfacial reaction between the iron in stainless steels and the carbon in diamonds [15-16]. This implies that nitrogen supersaturated stainless steels are suitable for a stamping mold material with high machinability in finishing and high hardness in stamping.

In the present paper, AISI420-J2 substrate is first employed to describe the nitrogen supersaturation behavior at 673 K by using the XRD (X-Ray Diffraction) and SEM (Scanning Electron Microscopy) – EDX (Electron Dispersive X-ray spectroscopy). Two types of mechanical machining tests as well as the precise finishing tests are utilized to demonstrate that this nitrogen

supersaturated layer of AISI420 alloy substrates is machined in the ductile mode by using the PCD-chipped cutting tools without chemical reaction between work and tool. The maximum surface roughness is controlled to be less than 10 nm by mechanically finishing this nitrided layer without damages to tools. Finally, the nitrided AISI420-base martensitic stainless steel substrate is machined to have the Fresnel textures and used as a mold for stamping the chalcogenide glass works to infrared, flat lenses. In addition to this high dimensional accuracy during imprinting, the demolding capacity is improved by the hydrophobic surface of nitrogen supersaturated AISI420 alloy mold.

Experimental Procedure

Low Temperature Plasma Nitriding System. A high-density plasma nitriding system was used in the following experiments. The system consisted of the vacuum chamber, the evacuation system, the DC (Direct Current)-RF (Radio Frequency) generator working in the frequency of 2 MHz, the mixture gas supply of N_2 and H_2, and, the heating unit located under the cathode plate, as illustrated in Figure 1a. In the vacuum chamber, the specimen was placed inside a hollow cathode setup on the cathode plate, which was electrically connected with DC generator. Both nitrogen and hydrogen plasmas were confined inside the setup to attain the nitrogen ion density of 3×10^{17} ions/m^3 under the optimum gas flow rate ratio [7, 17].
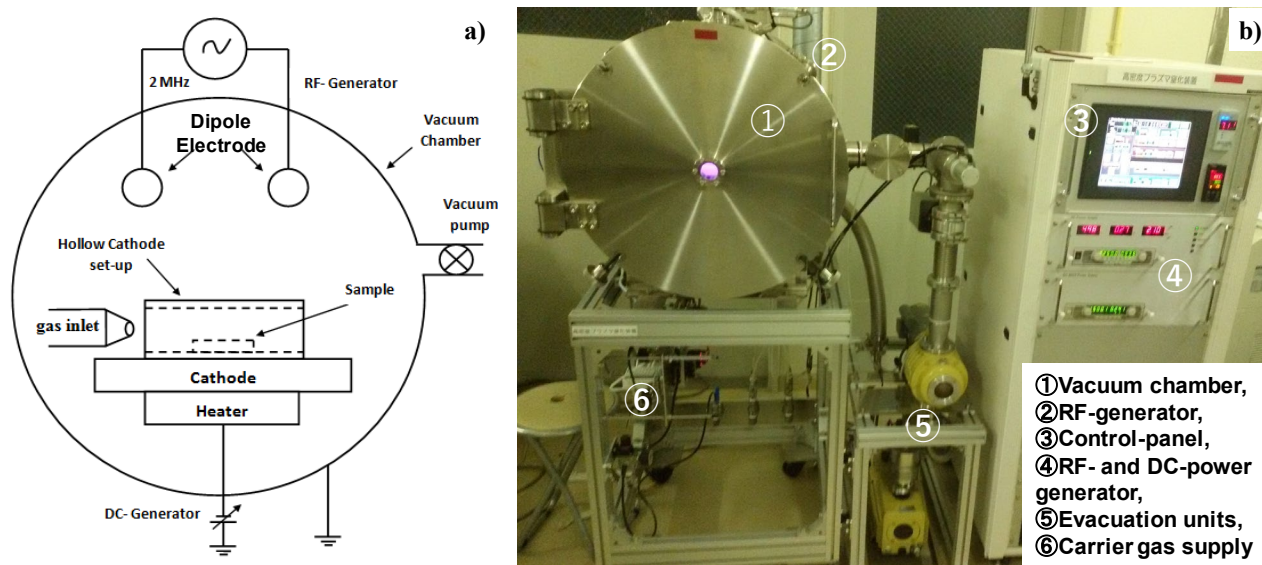

Figure 1. High density RF-DC plasma nitriding system. a) A schematic view of experiment setup for high density plasma nitriding, and b) overview of the high density RF-DC plasma nitriding system.

After placing the sample into the hollow cathode setup, the chamber was evacuated down to 0.5 Pa in pressure, and, then filled with the nitrogen gas with the flow rate of 160 ml/min until the pressure was constant by 60 Pa. After heating, the sample was pre-sputtered for 1.8 ks to remove any surfactants from its surfaces. This pre-sputtering process operated at 673 K using the DC discharge of 500 V in pure N_2 nitrogen gas by 60 Pa. After pre-sputtering, it was plasma nitrided for 7.2 ks (or 2h) and 14.4 ks (or 4h) at the holding temperature of 673 K or 400ºC by 60 Pa in pressure. The mixture of nitrogen and hydrogen gasses were supplied to have the ratio of 160 ml/min for nitrogen and 30 ml/min for hydrogen. During the nitriding, the RF-voltage and the DC-bias were constant by 250V and -500V, respectively. After the nitriding process, the sample was cooled down in the inert nitrogen atmosphere till 473 K to minimize the possibility of surface contamination.

Materials Characterization. A type AISI420-J2 martensitic stainless steel substrate and its derivatives were utilized as a substrate. Its standard chemical compositions were as follows; C < 0.15 mass%, Mn < 1 mass%, P < 0.04 mass%, S < 0.03 mass%, Si < 1 mass %, Cr < 12~14 mass%, and Fe in balance. SEM-EDX was utilized to analyze the cross-sectional microstructure and nitrogen

mapping of nitrided substrates at 673 K. Micro-Vickers hardness testing was employed to measure the hardness depth profile of nitrided specimen and molds.

Machinability Tests. Two types of mechanical machining tests were employed to describe the cutting behavior of the nitrogen supersaturated layer of ASIS420 by using the PCD-chipped cutting tool. In the former, a table-top machinability testing system (Multi-Pro; Takashima-Sangyo, Co., Ltd.; Tokyo, Japan) was employed to measure the transient of axial cutting forces (Fx, Fy and Fz) during the machining. A symmetric cutting tool with the PCD-chip was fixed to this simulator, as depicted in Figure 2.
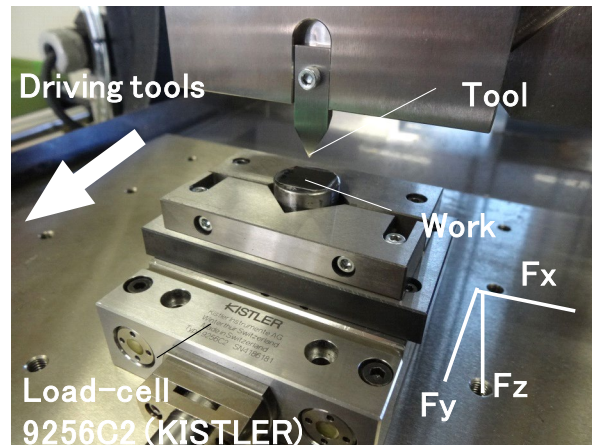

Figure 2. A machining process simulation to measure the transient of axial cutting forces (Fx, Fy, Fz) applied to the cutting tool during the machining of nitrided works.

The turning test was also employed to demonstrate that the nitrided layer was accurately machined by the PCD-chipped tool without chemical reaction between the diamond in chip and the nitrided stainless steel. In addition, the mechanical finishing test was utilized to prove that low surface roughness was attained by finishing the nitrogen supersaturated substrates.
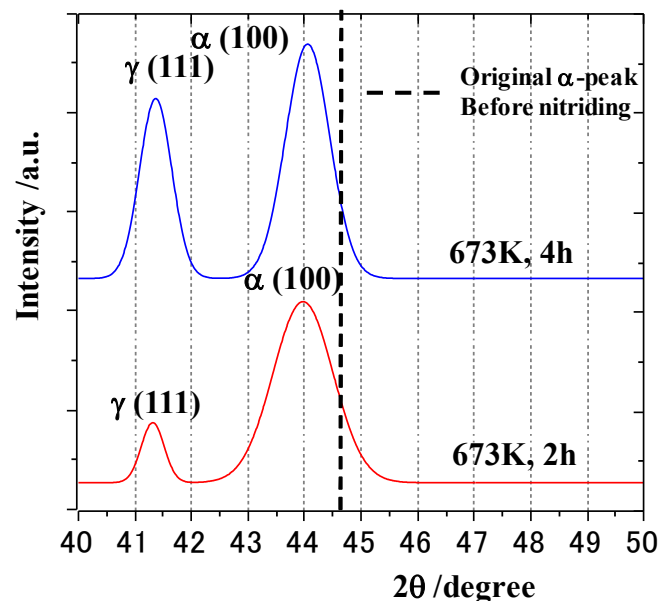

Figure 3. XRD analysis on the nitrided AISI420 specimen at 673 K for 7.2 ks (2h) and 14.4 ks (4h) by the Low Temperature Plasma Nitriding.

Experimental Results and Discussion

  Nitrogen supersaturation to AISI420 Specimens. The low temperature plasma nitriding process was characterized by XRD for various nitrided stainless steels [5-7]. The nitrided AISI420 specimens at 673 for 7.2 ks (or 2h) and 14.4 ks (or 4h) were prepared for XRD analysis. Figure 3 depicts their XRD profiles. No iron and chromium nitrides were detected except for two main peaks. One peak at $2\theta = 44°$ is an α-peak (100), which shifts from the original α-peak at $2\theta = 44.6°$ for AISI420. The other peak at $2\theta = 41.3°$ is a γ-peak (111). After the experimental works in Refs. [5-7] and [14-16] and the theoretical study in Ref. [18], the lattice expansion of α-iron by nitrogen atom occupation at the octahedral vacancy site in the iron cells is detected by the α-peak shift in the lower angle side of 2θ in the XRD analysis. That is, this XRD analysis in Figure 3 proves that nitrogen supersaturation advances into AISI420 specimen without significant precipitation of iron and chromium nitrides. As studied in [7, 11], the α- and γ-phase formation is commonly seen in the nitrided martensitic and austenitic stainless steels. This two phase formation in Figure 3, is induced by the local cluster-fluctuation in the nitrogen supersaturation under the different affinity of nitrogen atoms to iron, nickel and chromium atoms in the cells [19]. This nitrided AISI420 specimen was cut in half and polished for its cross-sectional analysis by SEM-EDX. Figure 4 depicts the cross-sectional microstructure and nitrogen mapping. The nitrided layer has fine crystal microstructure and high nitrogen concentration. The average grain size reaches 0.1 μm and the average nitrogen content is 3 to 4 mass%. This fine microstructure with high nitrogen content characterizes this nitrided layer of AISI420.
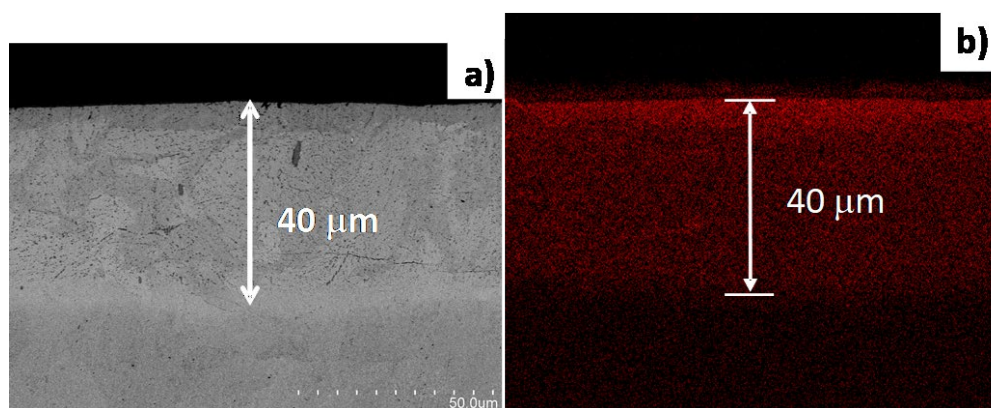

Figure 4. The cross-sectional microstructure and nitrogen mapping of nitrided AISI420-J2 stainless steels at 673K for 14.4 ks. a) A cross-sectional SEM image, and b) cross-sectional nitrogen mapping.
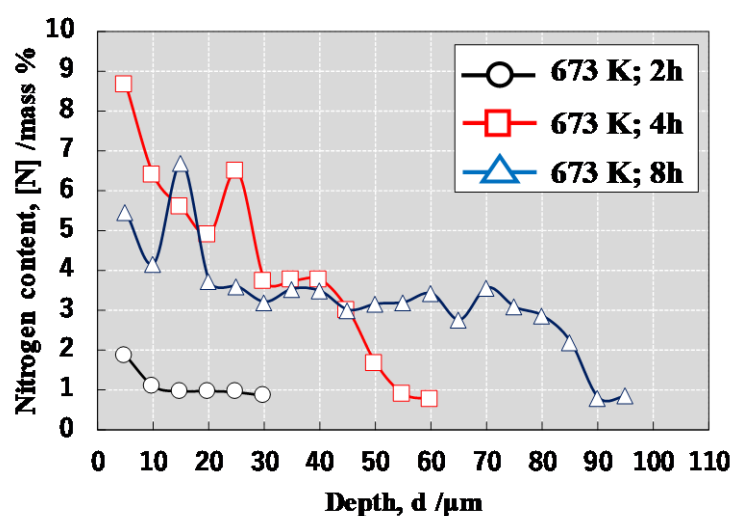

Figure 5. Comparison of the nitrogen content depth profiles for the nitrided AISI420-J2 specimen with increasing the nitriding duration.

The nitriding duration (τ) was increased from 7.2 ks (or 2 h) to 28.8 ks (or 8 h) to describe the nitrogen supersaturated layer formation in depth. Figure 5 depicts the nitrogen solute depth profiles at τ = 7.2 ks, 14.4 ks and 28.8ks, respectively. A nitrogen content plateau with constant nitrogen concentration by [N]p is commonly seen in these three profiles in Figure 5; e.g., [N]p = 1 mass% at τ = 7.2 ks, [N]p = 4 mass% at τ = 14.4 ks, and [N]p = 3 to 4 mass% at τ = 28.8 ks, respectively. This appearance of nitrogen content plateau proves that a sufficiently high amount of nitrogen solute content is present in nearly the whole nitrided layer to the depth of nitriding front end. After Refs. [7, 20], the nitrogen solute content exponentially decreases to the depth of nitrogen diffusing zones of the ion-nitrided and the radical-nitrided stainless steels and iron-chromium alloys. This exponentially decay of nitrogen solute content is attributed to the fact where the inner nitriding mechanism in those conventional nitriding processes is mainly governed by the nitrogen body-diffusion. On the other hand, in this low temperature plasma nitriding, the grain size refinement is induced by the nitrogen supersaturation to form the fine zone- and grain-boundaries into the nitrided layer, as explained in [7, 21-22]. These boundaries work as a network of nitrogen diffusion so that a sufficient amount of nitrogen content is preserved in the nitrided layer.

When τ > 14.4 ks, higher nitrogen solute content than 3 mass% or 12 at%, is preserved through the nitrided layer as shown in Figure 5. After [18, 23], most of iron atoms in the α-iron cells are attracted to each nitrogen interstitial atom in its first and second neighboring ranges. That is, the original a-iron celled system is converted to an assembly of the bound clusters among iron and nitrogen atoms. This unique microstructure in Fe-N system with high nitrogen content is so stable that other element atoms have no rooms to react to these iron atoms in this microstructural constraint. Hence, the nitrogen supersaturated AISI420 alloys can be machined by the diamond-coated or diamond-chipped tools since the carbon atoms in diamond never react with the bound iron atoms to nitrogen solute atoms.

This improvement of machinability by the nitrided AISI420 alloy substrate is demonstrated by the machining simulation, the turning test and the finishing experiments in what follows.

Dry machining test of nitrided AISI420 base substrates. The machinability test was employed to describe how the nitrogen supersaturated layer was cut in by using the PCD-chipped tool. This testing was performed by varying the starting point depth and the machining direction. When the starting point is included in the nitrided layer, as shown in the SEM image in Figure 6, no cracks and defects were seen in the machined trace toward the surface; this machining takes place in the ductile mode. In general, as reported in [24], the machined surface in the brittle mode has a series of cracks along the cutting path across the nitriding front end. While a smooth fine trace is left on the machined surface in ductile mode within the nitrided layer. This SEM image on the cutting path without any cracks proves that no adhesives are induced on the cutting path by the chemical reaction between the carbon in PCD and the iron in the nitrided layer of AISI420.

The transients of three axial cutting forces were also measured during the above machining process. The x-axial force, Fx is nearly zero and insensitive to this machining process. Consider the experiment setup in Figure 2; the PCD-chipped tool was driven in the vertical direction to the x-axis. Hence, Fx ~ 0 in Figure 6 proves that the machining takes place in the y-z plane under this experimental setup. The measured axial cutting forces of Fy and Fz monotonously decrease from the depth of nitrided layer to its surface. No significant fluctuations are detected in these transients. Since the cutting forces are sensitive to the dissimilar zones and secondary-phase precipitates, this monotonous decrease of Fy and Fz reveals that no inhomogeneous nitride precipitates are present in the nitrided layer to induce the peak-to-valley fluctuations in Figure 6.

Since the cutting area monotonically decreases with the machining distance, both Fy and Fz also monotonously decreases with the distance. This suggests that the plastic flow resistivity or the shear yield stress pf nitrided AISI420 alloys might be constant. That is, the machinability of this nitrided AISI420 alloys is just the same as the capacity to cut in the homogeneous work materials such as the un-nitrided AISI420 alloys. No special technique is necessary to shape and finish this nitrided AISI420 alloys by machining. A normal machining theory is true to this cutting process.
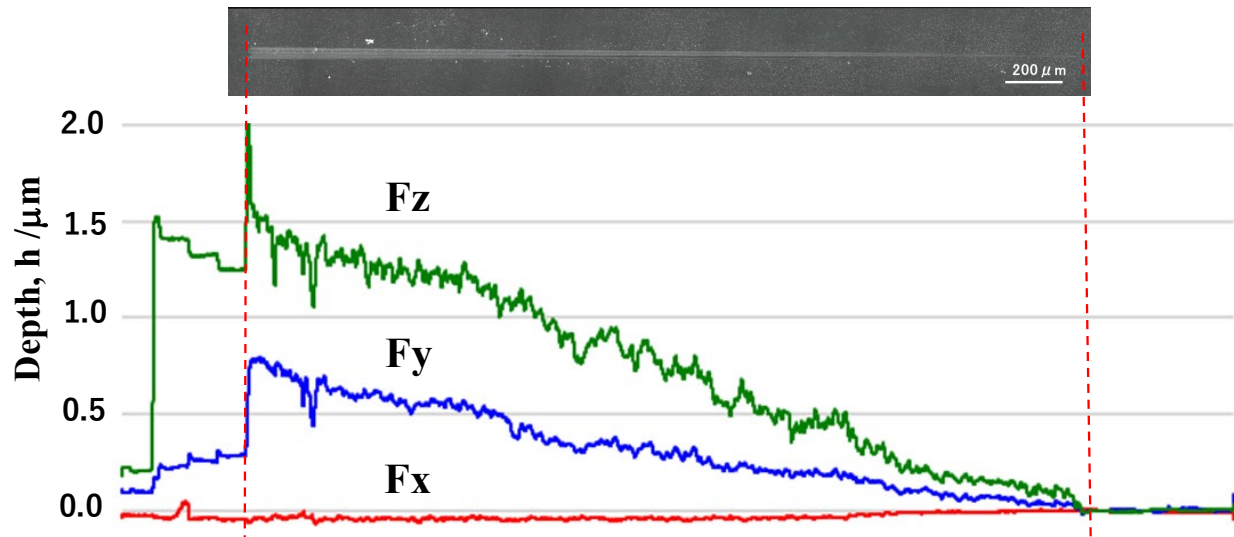
Figure 6. Mechanical machining behavior from the depth of nitrided layer to its surface. The cutting path was observed by SEM. The transients of axial cutting forces were in situ monitored during the machining.
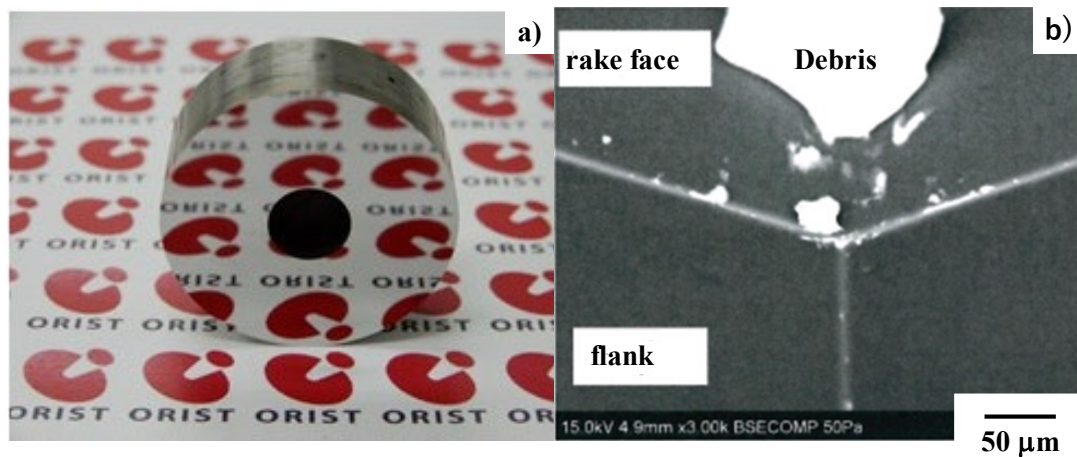

Figure 7. Turning test of the nitrided AISI420 substrate with the constant feed and machining speeds. a) Mirror-shining surface after turning test by 90 m, and, b) the edge condition of PCD-chip.
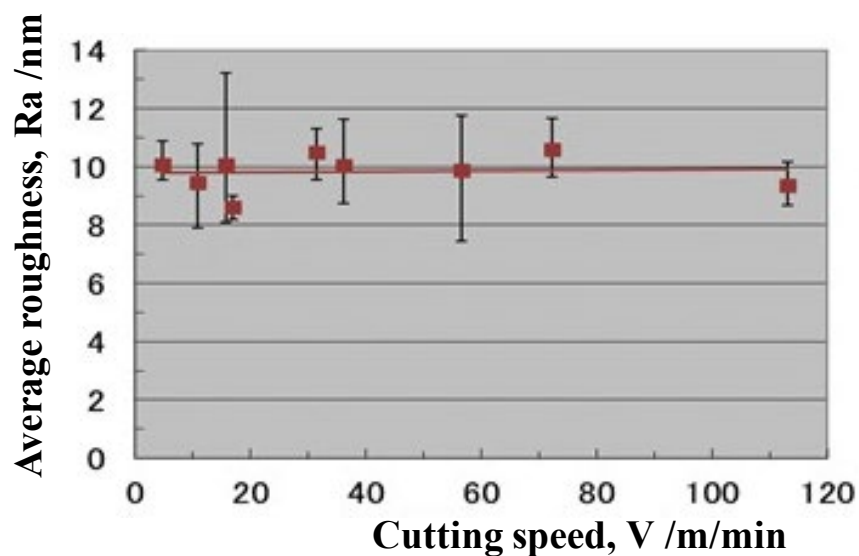

Figure 8. Variation of the average roughness with increasing the cutting speed in finishing the nitrided AISI420 alloy mold substrate.

The turning test was performed to demonstrate that the nitrogen supersaturated AISI420 alloy substrate was machined to form the smooth surfaces. Figure 7a depicts the snap-shot of machined AISI420 substrate after turning it at the distance of 90 m. The mirror-shining surface proves that no tearing occurs on the machined surface even after long-distance turning and that every cutting process advances in the ductile mode in similar manner to the smooth cutting transients in Figure 6. In correspondence to the occurrence of brittle mode machining along the cutting path across the nitriding front end or from the un-nitrided depth to the nitrided layer in the machinability test, the tears were observed on the nitrided zones with lower nitrogen content than 1 mass% in this turning test.

Figure 7b shows the PCD-chip edges after turning in 90 m. No wears were seen on each edge. This proves that no tears on the machined work surface is just corresponding to no wears on the PCD-chip edges. That is, no galling reactions between carbon in PDC and iron in the nitrided AISI420 are induced into the nitrogen supersaturated AISI420 substrate with the high nitrogen solute concentration as predicted before.

Figure 9. Mold-stamping of the Fresnel textures onto the chalcogenide lens for infrared camera and elements by using the nitrided AISI420 mold after finishing and texturing.

This well-defined surface of machined AISI420 substrate significantly reflects on the finishing behavior to reduce the surface roughness for stamping mold of oxide and metalloid glasses. In particular, the low roughness mold surface is indispensable for stamping the micro-textures of DOE (Diffraction Optical Element) onto the chalcogenide glass works. The finishing experiment of nitrided AISI420 molds was performed with varying the cutting speed.

In general, the surface roughness reduces with increasing the cutting speed [25]. In case of finishing the mold surface, the machining speed varies by itself from cutting the center of mold to its end. Hence, the high quality mold surface must be preserved even by varying the machining speed in one to two orders. The stylus-based profilometer was laser employed to measure the finished surface roughness. Figure 8 proves that the average surface roughness is sustained to be 10 nm or less than even by varying the cutting speed from 5 m/min to 115 m/min. This high quality mold surface by finishing becomes a platform to build up the DOE such as the Fresnel pattern for flat lens by using the PCD-chipped and CBN-chipped tools and to further reduce the surface roughness for laser mirrors.

Precise stamping by using the nitrided AISI420 alloy molds. A micro-texture for the Fresnel lens was cut in to the nitrided AISI420 mold after finishing in the above. This mold was utilized to form the Fresnel lens profile onto the chalcogenide glass work by warm stamping. A mold-stamped work is shown in Figure 9. The tailored Fresnel microtextures are accurately imprinted onto the chalcogenide glass work. This demonstrates that the flat infrared lens is fabricated by the mold-stamping with the use of the finished, nitrided-AISI420 alloy mold.

In general, the oxide and metalloid glasses are easy to adhere to the mold substrate surface. In particular, the regular microtextures such as the Fresnel pattern are apt to induce the galling of those glass works. In order to prevent the mold surface from this chemical galling of glasses, the mold surface must have low surface energy. The wettability test is employed to measure the contact angle

on the three mold surfaces and to explain the superiority to the nitrided AISI420 alloy substrate in the mold stamping.

The original AISI420 alloy mold surface is hydrophilic in similar manner to most of metals and alloys, as seen in Figure 10a. That is, the AISI420 alloy molds have higher surface energy enough to be adherent to glass works without the protective coatings. However, the NiP-coating has nearly the same contact angle as the original AISI420 alloys, as noticed in Figure 10b. This high surface energy intrinsic to NiP coating induces the severe adhesion to the chalcogenide glasses under the triggering by its crystallization during the mold-stamping.
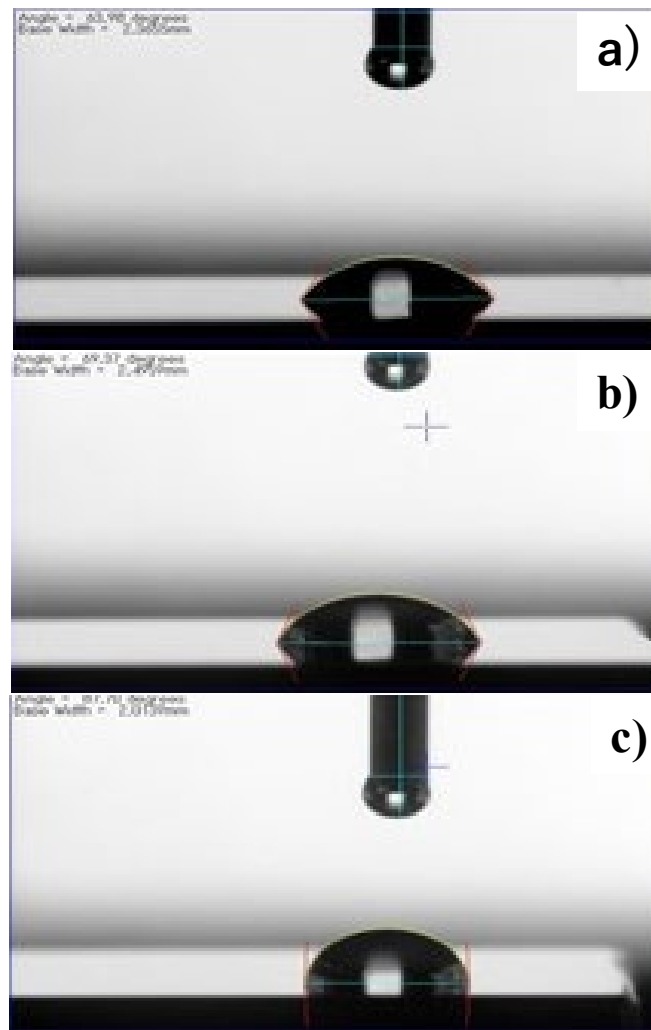

Figure 10. Surface property control by changing the mold substrate. a) Untreated AISI420 mold substrate, b) NiP-coated mold substrate, and c) nitrogen supersaturated AISI420 mold substrate.

Figure 10c depicts the contact angel of pure water on the surface of nitrogen supersaturated AISI420 alloy molds. Since the measured contact angle is more than 90°, the original hydrophilic surface in Figure 10a changes to be hydrophobic only by nitrogen supersaturation to AISI420 alloy mold. This lower surface energy state of nitrided AISI420 alloy improves the demolding capacity in the mold stamping. The chemical adhesion of glass preforms to the mold surface has been an engineering issue to lower the productivity in mold stamping of metalloid glasses including the chalcogenide glasses. No adhesive surface area in Figure 9 proves this hydrophobic mold surface has much low possibility to induce the chemical galling even to chalcogenide glass works.

Let us consider why the nitrided AISI420 alloy mold substrate has lower surface energy. The untreated AISI420 alloy surface is still metallic since iron has unbound electrons even at the presence of chromium and other elements. When the interstitial nitrogen atoms are enriched at the surface,

most of iron atoms are attractive to these nitrogen solute atoms so that iron atoms at the vicinity of surface are bound among the attracted Fe - N clusters. This stable microstructure with the chemical inertness reduces the surface energy; the original hydrophilic mold surface changes to be hydrophobic by the high content nitrogen supersaturation into stainless steels.

Summary

The nitrogen supersaturated martensitic stainless steel type AISI420 mold substrate has sufficiently high surface hardness and thicker nitrided layer than 80 μm, has sufficiently higher content of nitrogen solute than 4 mass% in uniform within the nitrided layer, and has much lower surface energy than the original AISI420 and NiP-coated one. Its machinability in the ductile mode with monotonous cutting force transients, proves that no iron and chromium nitride precipitates are present to hinder the ductile-mode cutting behavior and that no tiny tears are induced even on the PCD-chip edges by the chemical reaction between the iron in the nitrided AISI420 and the carbon in PCD. Mirror-like surface is attained by turning the nitrided AISI420 alloy substrates. This demonstrates that the nitrogen supersaturated AISI420 alloy can be utilized as a mold to imprint the high quality mold surface to the oxide and metalloid glass preforms by mold-stamping, instead of the NiP and NiWP coatings. In particular, the chalcogenide glass, which is easy to adhere to the metallic mold surface, is formed to a flat, infrared lens element without tiny tears on its surface by the mold-stamping.

In the conventional nitriding processes, fine precipitation of iron and chromium nitrides has a role of hardening process. The nitrogen diffusing layer is thin and the nitrogen content is insufficient to improve the machinability by nitriding. In the present high density plasma nitriding, the nitrogen content plateau thickness with 3-4 mass% reaches to 80 μm, and it has high average hardness of 1400 HV. This unique nitrogen solute depth profile is linked with high mechanical machinability by the diamond tools. The constituent iron atoms in the nitrided layer are attractive to the nitrogen interstitial atoms so that every iron atom is bound to these nitrogen interstitials. This highly bound state in Fe (Cr) – N system results in the high strength and hardness, the high machinability by no reactions between iron and carbon in diamond, and the high demolding capacity by hydrophobicity.

Acknowledgements

References

[1] K. M. Budinski, J. C. PulverJayson, J. N. Eugene. G. Hill, D. A. Richards, Glass mold material for precision glass molding. US-Patent with US6363747B1 (2001).

[2] Q. Yu, T. Zhou, Y. He, P. Liu, X. Wang, Y. Jiang, J. Yan, Annealed high-phosphorous electroless Ni-P coatings for producing molds for precision glass molding. Mater. Chem. Phys. 262 (32) (2021) 124297.

[3] K. Saito, Introduction to ion nitriding in Hokunetsu. (2018). http://hokunetsu.com/ products/003/ (retrieved at 2021/11/16).

[4] H. Aghajani, S. Behrangi, Pulsed DC glow discharge plasma nitriding. In: Plasma Nitriding of Steels, Springer (2016) 71-125.

[5] T. Bell, Surface engineering of austenitic stainless steel. Surf. Eng. 18 (2002) 415-422.

[6] H. Dong, S-phase surface engineering of Fe-Cr, Co-Cr and Ni-Cr alloys. International Materials Reviews. 55(2) (2011) 65-98.

[7] T. Aizawa, Low temperature plasma nitriding of austenitic stainless steels. Ch. 3 In: Stainless Steels. IntechOpen, London, UK (2018) 31-50.

[8] Lu S.; Zhao X., Wang S., Li J., Wei W., Hu J., Performance enhancement by plasma nitriding at low gas pressure for 304 austenitic stainless steel. Vacuum. 2017; 145: pp. 334-339.

[9] T. Aizawa, T. Shiratori, T. Komatsu, Micro-/nano-structuring in stainless steels by metal forming and materials processing. Ch. 5 In: Electron Crystallography. IntechOpen, London, UK (2020) 101-122.

[10] F. Borgioli, E. Galvanetto, T. Bacco, Low temperature nitriding of AISI300 and 200 series austenitic stainless steels. Vacuum 12 (2016) 51–60

[11] A. Farghali, T. Aizawa, T. Yoshino, Microstructure/mechanical characterization of plasma nitrided fine-grain austenitic stainless steels in low temperature. J. Nitrogen 2 (2021) 244-258.

[12] T. Katoh, T. Aizawa, T. Yamaguchi: Plasma assisted nitriding for micro-texturing onto martensitic stainless steels. Manufacturing Review 2 (2) (2015) 1-7.

[13] D. J. Djoko, T. Aizawa, Formation of expanded martensite in plasma nitrided AISI420 stainless steel. Pro. 8th SEATUC Conf. (Johor-Balu, Malaysia; March 2014) (CD-ROM).

[14] A. Farghali, T. Aizawa, Nitrogen supersaturation process in the AISI420 martensitic stainless steels by low temperature plasma nitriding. ISIJ International. 58 (3) (2018) 401-407.

[15] T. Aizawa, T. Fukuda, Microstructure and micro-machinability of plasma nitrided AISI420 martensitic stainless steels at 673 K. Top-5 Cont. to Mater. Sci. 6th Ed. Avid Science (2019) 2-23.

[16] T. Aizawa, H. Morita, T. Fukuda, High machinability of plasma-nitrided HPM80 dies at 673K by PCD-tools for hot mold-stamping. Procedia Manufacturing 47 (2020) 725-731.

[17] T. Aizawa, I, Rsadi, E. E. Yunata, High density RF-DC plasma nitriding under optimized conditions by plasma-diagnosis. J. Appl. Sci. (2021) (in press).

[18] C. Domain, C. S. Becquart, J. Foct, Ab initio study of foreign interstitial atom (C, N) interactions with intrinsic point defects in a-Fe. Phys. Rev. B 69 (2004) 144122.

[19] T. Aizawa, T. Shiratori, T. Yoshino, Y. Suzuki, T. Komatsu, Nitrogen supersaturation of AISI316/316L/316LN stainless steels at 673 K for hardening and microstructure control. Ch. In: Stainless Steels, InTechOpen, London, UK (2021) (in press).

[20] Y. Hiraoka, K. Inoue, Prediction of nitrogen distribution in steels after plasma nitriding. Denki-Seiko 86 (2010) 15-24.

[21] T. Aizawa, S-I. Yoshihara, Inner nitriding behavior and mechanism in stainless steels at 753 K and 623 K. SEATUC J. Sc. Eng. (SJSE) 1 (2019) 13-20.

[22] T. Aizawa, T. Yoshino, K. Morikawa, S-I. Yoshihara, Microstructure of plasma nitrided AISI420 martensitic stainless steel at 673 K. J. crystals 9 (2), 60 (2019) 1 - 10.

[23] Y. Imai, T. Murata, M. Sakamoto, High nitrogen steels. (2005) Agune.

[24] B. R. Lawn, O. Borrero-Lopez, H. Huang, Y. Zhang, Micromechanics of machining and wear in hard and brittle materials. J. Amcer. Soc. 104 (1) (2021) 5-22.

[25] P. Parhad, A. Likhite, J. Bhatt, D. Peshwe, The effect of cutting speed and depth of cut on surface roughness during machining of austempered ductile iron. Trans. Indian Institute Metals. 68 (2015) 99-108.